ELSEVIER

Biophysical Chemistry 121 (2006) 224–233

Biophysical Chemistry

http://www.elsevier.com/locate/biophyschem

Difference in the effects of surfactants and albumin on the extent of deaggregation of purpurin 18, a model of hydrophobic photosensitizer

Padmaja P. Mishra, Anindya Datta *

Department of Chemistry, Indian Institute of Technology Bombay, Powai, Mumbai 400 076, India

Received 28 October 2005; received in revised form 23 January 2006; accepted 24 January 2006
Available online 28 February 2006

Abstract

Absorption, fluorescence and light scattering techniques have been used to monitor the deaggregation of purpurin 18, a model of hydrophobic photosensitizers for photodynamic therapy, in aqueous micelles, microemulsions and human serum albumin. The aggregates present in the neat aqueous solvents are found to undergo deaggregation in these media to different extents. Aqueous micelles and microemulsions are found to induce a complete deaggregation whereas the process is only partial in albumins. This could be an indication of the fact that such hydrophobic photosensitizers are likely to be aggregated in the blood stream, but are probably in monomeric form, upon cellular uptake. The formation of surfactant-induced aggregates at intermediate concentrations of the positively charged CTAB is also observed and is explained in the light of electrostatic interactions between the fluorophore and the surfactant.

Keywords: Purpurin 18; Surfactant; Albumin; Deaggregation

1. Introduction

The interaction of porphyrins and chlorins with surfactant assemblies and biomolecules is interesting because of the relevance of such complexes in photosynthesis, oxygen transport, electron transfer processes and photodynamic therapy (PDT) [1–9]. In the last of these applications especially, the interaction is of utmost importance as hydrophobic photosensitizers tend to form aggregates in aqueous solutions [10–12], which leads to their smaller photodynamic activity while hydrophilic photosensitizers display decreased cellular uptake, target less photosensitive subcellular sites and are rapidly cleared in vivo [7,8]. Consequently, pre-incorporation in suitable delivery vehicles is often required to solubilize the aggregates and to facilitate cellular uptake [1,3,6,13–16]. Thus, it is essential to study the effect of the interaction with biomolecules and surfactant assemblies on the aggregation behavior of the photosensitizers.

In this context, there has been a flurry of activity in the study of aggregation and deaggregation processes of chlorin derivatives [4–6]. It is important to study the effect of pH on such processes, as the extracellular pH of the tumor cells is reported to be somewhat lower than the physiological pH and this is proposed to be an important parameter that might govern the selective localization of drugs with ionizable side chains in the tumor cells [17]. We have earlier observed the aggregation of chlorin p_6 in the pH range 7–3, due to successive protonation of the anionic carboxylic groups and the ring nitrogens, similar to the observations in earlier studies [10–12]. Fluorescence quenching in these aggregates of chlorin p_6 is static in nature [4]. Recently we have reported the preliminary fluorescence monitoring of pH dependence of chlorin p_6-surfactant aggregates, which have been found to form with the cationic CTAB at pH 7 and 5 and with the anionic SDS at pH 3 [18]. An effect of pH on the cellular uptake as well as in liposome-binding of chlorin p_6 has been observed [5,6]. A similar effect is observed only for certain kinds of cell lines whereas for others, the uptake is determined by diffusional processes and shows no effect of pH. Very recently, we have observed a modification of the acid–base equilibrium of chlorin p_6 that occurs upon its incorporation

* Corresponding author. Fax: +91 22 2572 3480.
E-mail address: anindya@chem.iitb.ac.in (A. Datta).

0301-4622/$ - see front matter © 2006 Elsevier B.V. All rights reserved.
doi:10.1016/j.bpc.2006.01.009

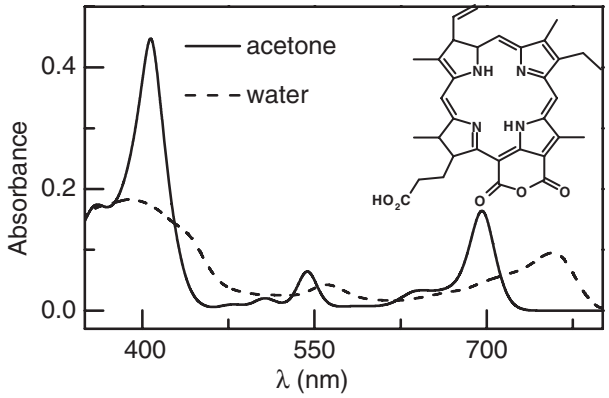

Fig. 1. Absorption spectra of 7 μM purpurin 18 in acetone (—) and in water (- - -). The inset shows the structure of purpurin 18.

in Cremophor EL, a drug delivery vehicle [19]. In continuation of this series of ongoing studies, we have performed a fluorescence investigation on the effect of micelles, reverse micelles and albumins on the deaggregation of purpurin 18, which is the precursor to chlorin p_6 in its preparation from chlorophyll. The only structural difference between chlorin p_6 and purpurin 18 is that, instead of three ionizable carboxylic groups in the former, there is a carboxylic group and an anhydride ring in the latter. This small difference in structure has rather important effect on the properties of purpurin 18, making it considerably more hydrophobic in nature, causing it to aggregate at neutral pH, with broad absorption peaks at 400 nm and 758 nm (Fig. 1). The compound is likely to have a unit negative charge, as the carboxylic acid group that is separated by two carbon atoms from the ring system is expected to behave like an aliphatic carboxylic acid and have a pK_a of ~4.8 [20]. In an aqueous solution, no emission is observed for excitation at either of the bands. The principal motivation of this study is to investigate the difference in the binding of the probe with the surfactant assemblies and the albumin and to explore the relative efficiencies of these media as far as the deaggregation of the hydrophobic fluorophore is concerned, as this is an important issue that determines the photodynamic efficacy of the photosensitizer.

2. Experimental section

2.1. Materials

Purpurin 18 is prepared from dry spinach leaves following literature procedure [21]. Its purity is tested by thin layer chromatography (TLC), elemental analysis, mass spectroscopy and superimposability of the absorption and excitation spectra. All the experiments have been carried out with 7 μM solutions of the fluorophore in phosphate buffered saline (PBS) at pH 7.4. AR grade cetyltrimethylammonium bromide (CTAB) and sodium dodecyl sulfate (SDS) have been recrystallized from alcohol–water mixtures. Aerosol OT from Sigma is purified by literature procedure [22]. Human serum albumin (HSA) from Sigma is used without further purification. All other chemicals are from E-Merck, Mumbai, India or SD Fine Chemicals, Mumbai, India.

2.2. Absorption and fluorescence measurements

The absorption and fluorescence (λ_{ex}=407 nm) spectra have been recorded on JASCO V570 and Perkin Elmer LS55 spectrophotometers, respectively. Fluorescence quantum yields (ϕ_f) are calculated using tetraphenyl porphyrin (TPP) as the standard (ϕ_f=0.11) [23]. Time-resolved fluorescence measurements have been carried out at magic angle (54.7°), with λ_{em} of 710 nm, on an IBH Fluorocube picosecond time correlated single photon counting (TCSPC) setup, which uses a 406 nm diode laser as the excitation light source and a resolution of 7 ps per channel. The decays, which are not monoexponential, are fitted as multiexponential functions and the average lifetime is calculated from the relation $\tau_f=\Sigma_i a_i\tau_i$. The radiative rates ($k_R$) and the nonradiative rates (k_{NR}) are calculated by using the formulae $k_R=(\phi_f/\tau_f)$ and $k_{NR}=((1-\phi_f)/\tau_f)$ respectively. A concentrated stock solution of purpurin 18 is prepared in acetone, from which 2 μl are added per 1 ml of potassium phosphate buffer in Millipore water, to prepare a 7 μM solution, for the spectroscopic studies. The volumes are measured by micropipettes. To a part of this solution, surfactants/protein are added and the solution is allowed to equilibrate for 1 h. From this stock solution of surfactant or protein, aliquot are added to 7 μM purpurin 18 solution to keep the concentration of fluorophore constant and to vary the concentrations of surfactants or protein. The readings are taken after equilibrium, until the spectra are superimposable in three consecutive readings.

2.3. Light scattering experiments

Resonance light scattering (RLS) spectra are recorded by the Perkin Elmer LS55 spectrophotometers in the synchronous scan mode with zero offset as described by Pasternack et al. [24,25]. Each titrated spectrum is base line corrected as described elsewhere [24,25]. Experiments have been carried out at room temperature (25±2 °C). All experimental data are the average of at least three independent experiments.

Dynamic light scattering (DLS) measurements have been performed using a BI-MAS multiangle sizing Zeta Plus instrument, in which the light source used is a 15 mW continuous solid state laser of 660 nm. Intensity of the scattering light from the sample solution is measured in perpendicular direction to that of the incident laser light by an Avalanche Photodiode (APD). The measurements have been performed using the standard 1 cm quartz cuvette, which allows sufficiently large volume for proper mixing of the components. Essentially the instrument measures the diffusion coefficient (D) of the dispersed aggregates and evaluates the hydrodynamic diameter (d_h) in terms of Stokes–Einstein equation,

$$d_h = \frac{kT}{3\pi\eta D} \quad (1)$$

where η, k and T are the viscosity coefficient of the medium, the Boltzmann constant and the absolute temperature respectively.

All the above experiments are carried out by taking 2 ml of solutions of purpurin 18 in buffer initially in a quartz cuvette and subsequently adding either of the surfactants or HSA, to get a final volume of 3 ml. During the experiments, the temperature is tried to be kept at 25 °C. For the light scattering experiments, the solutions are prepared in Millipore water and further, to avoid the presence of any dust particles, the sample solutions were centrifuged at 10,000 rpm for 30 min.

2.4. Cryo-TEM and SEM imagings

The aggregation morphology is monitored by scanning electron microscopy (SEM) and transmission electron microscopy (TEM) techniques by using a FET Quanta-200 instrument and a cryo-based TEM of model TECHNAI 20-G instrument respectively. For SEM imaging, a droplet (~1 μL) of the sample is kept on a stainless steel stub and the imaging analyses have been done at low vacuum (0.98 Torr). For the TEM imaging, a droplet of the sample (~1 μL) is placed on the sample holder and plunged into liquid nitrogen at high speed for fast cooling to avoid further recombination of the aggregates to form larger aggregates.

2.5. Determination of constant of association (K_a) with surfactants

The association constant K_a is then calculated from the absorption spectra using the following relationship [26,27]:

$$A = A_f^0 + \frac{A_b^0 - A_f^0}{\frac{1}{K_a([S]_0 - \mathrm{cmc})^N} + 1} \quad (2)$$

where A, A_f^0 and A_b^0 are the absorbances in a given concentration $[S]_0$, zero concentration and maximum concentration of the surfactant, respectively. cmc is the critical micellar concentration and N is the micelles to fluorophore stoichiometry, which is kept one during the analysis for making the analysis simple, as the concentration of fluorophore is the order of magnitude lower than that of the surfactant after the micelles are formed.

2.6. Determination of binding constant with protein and the number of binding sites

A plot of $(A_0/\Delta A)$ vs. $(1/[P]_T)$ is constructed, where A_0 is the absorbance of 7 μM purpurin at 705 nm in the absence of protein and ΔA is the change in absorption at an HSA concentration of $[P]_T$. A_∞, the absorbance of the sample at infinite protein concentration is determined from the ordinate intercept of this plot. Hence, log $[P]_F$ is plotted against log $\{[A_0 - A_C]/(A_C - A_\infty)\}$ (Chipman plot), where $[P]_F$ is the free protein concentration and A_C is the absorbance of the sample. The abscissa intercept of this plot yields the pK_b for the purpurin 18–HSA interaction according to the following relationship [28,29]:

$$\log\frac{A_0 - A_C}{A_C - A_\infty} = \mathrm{p}K_b + \log\left\{[P]_T - [L]_T\frac{A_0 - A_C}{A_C - A_\infty}\right\} \quad (3)$$

where $[L]_T$ is the total concentration of the purpurin 18 and $[P]_F$, the free protein concentration is given by:

$$[P]_F = \left\{[P]_T - [L]_T\frac{A_0 - A_C}{A_C - A_\infty}\right\} \quad (4)$$

3. Results and discussion

3.1. Disruption of purpurin 18 aggregates in water by surfactants

Purpurin 18, being highly hydrophobic in nature, aggregates in PBS at pH 7.4 [21]. This is manifested in the red-shifted, broad absorption peaks at 560 nm and 760 nm, compared to those in acetone (540 nm and 695 nm respectively), for example (Fig. 1). From the SEM and TEM images of these aggregates, the diameter turns out to be in the range of 650 nm to 1200 nm (Fig. 2a, b), which is comparable to the size of the aggregates of porphyrins, determined from the electron microscopes, reported earlier by other groups (200 nm–800 nm) [11]. The disruption of these aggregates on addition of CTAB, even at submicellar concentrations, is reflected in a decrease in the number density as well as size of the particles in the SEM images at submicellar

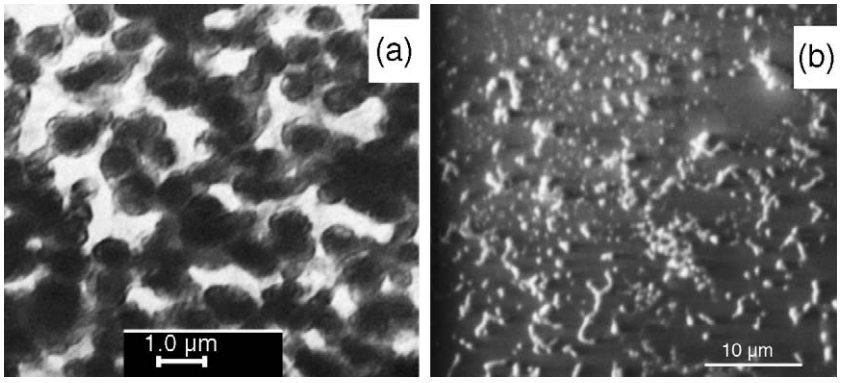

Fig. 2. (a) TEM and (b) SEM images of the aggregates of 7 μM purpurin 18 in PBS of pH 7.4.

concentrations of CTAB. Beyond the cmc, which is 0.9 mM for CTAB, a large number of aggregates are observed in the images, with typical diameters of 12 nm. These aggregates are the CTAB micelles, as their dimensions match those of the micelles reported earlier [30]. The disruption of the aggregates is accompanied by marked changes in the absorption spectra. The broad absorption bands decrease in intensity and new peaks emerge at 406 nm and 702 nm, with an isosbestic point at 718 nm (Fig. 3a). These bands are characteristic of monomeric purpurin 18 (Fig. 1). The ratio between absorbances at 758 nm and 702 nm decreases gradually until a concentration of 1 mM of CTAB (which is near the cmc of CTAB) and remains unchanged thereafter with a value of almost zero, signifying complete deaggregation of purpurin 18 in micelles (Fig. 4a). It is notable that a small peak at 775 nm appears at a CTAB concentration of 0.06 mM and remains perceivable up to a concentration of 0.1 mM, after which it diminishes and finally vanishes at a CTAB concentration of 0.4 mM. With SDS, the peak at 758 nm decreases with a concomitant development of a new peak at 702 nm without the development of any other band at intermediate concentrations. An isosbestic point is observed at 723 nm. The Soret band also becomes narrower with a peak shift to 412 nm at a concentration about the cmc (8 mM) of SDS. The peak at 758 nm completely disappears at an SDS concentration of 12 mM (Fig. 3b), indicating a complete disruption of aggregates similar to that with CTAB. Thus, it seems that the intermediate small band in CTAB could have arisen due to the formation of some premicellar aggregate of a

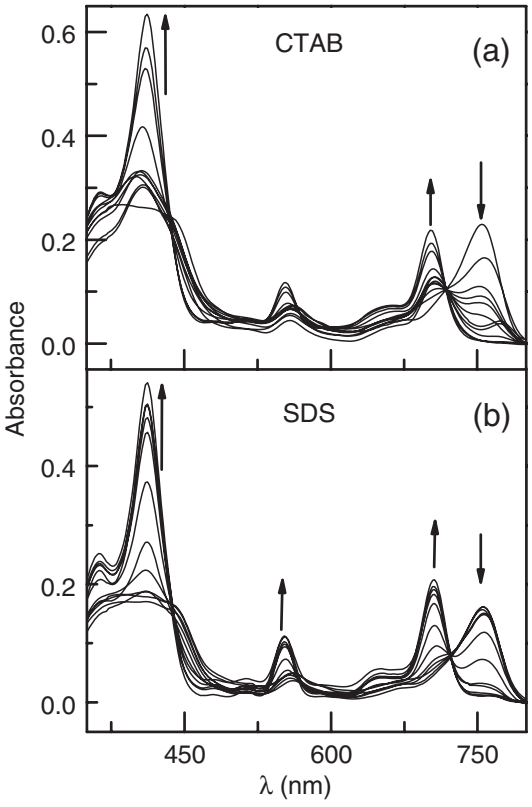

Fig. 3. Absorption spectra of 7 μM purpurin 18 at pH 7.4 at different concentrations of (a) CTAB (0 to 10 mM) and (b) SDS (0 to 30 mM).

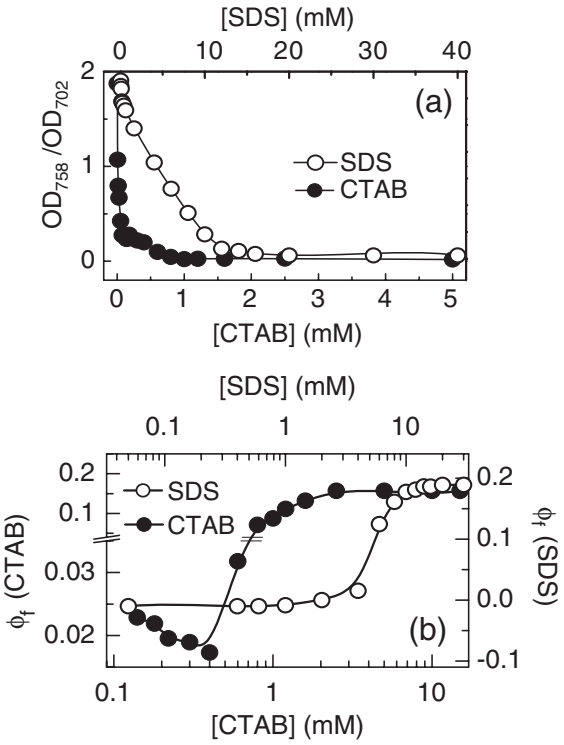

Fig. 4. Variation of (a) OD_{758}/OD_{702} and (b) fluorescence quantum yield (ϕ_f) of 7 μM purpurin 18 at pH 7.4 with increasing concentrations of CTAB and SDS.

different kind due to the interaction of the single negatively charged carboxylic group present in purpurin 18 molecule and the positively charged surfactant. In SDS such electrostatic interactions are not possible and the electrostatic factor is not favorable for such aggregation. With both the surfactants, the ratio between the absorbance at 758 nm and 702 nm decreases to almost zero at the cmc (Fig. 4a). However, the decay of the ratio is much steeper with CTAB, presumably because the self-aggregates have an additional channel of disruption through the formation of surfactant-induced aggregates with CTAB. The more gentle slope in the plot for SDS could also be explained by the consideration of the charges on the head groups of the surfactants. The negatively charged head groups of SDS molecules are likely to repel the like-charged purpurin 18 molecules, thereby hindering the process of the disruption of the self-aggregates. On the other hand, the positively charged head group of CTAB molecules can be expected to attract the fluorophore molecule and thereby, offers an electrostatic assistance to the disruption of the aggregates, which is primarily driven by the hydrophobic effect.

Purpurin 18 does not fluoresce at all at pH 7.4, irrespective of the wavelength of excitation. On addition of CTAB, there is an onset of emission at a surfactant concentration of 0.14 mM. The emission quantum yield (ϕ_f) exhibits an abrupt increase at the cmc of CTAB and reaches a plateau beyond a concentration of 2 mM (Fig. 4b). Similar sigmoidal variation is obtained with SDS with the point of inflection around its cmc. In case of CTAB, there is a small, unlike decrease in quantum yield whereas there are no such observations with SDS. This reinforces the contention about the formation of

some nonradiative surfactant-induced aggregates at the intermediate concentrations of CTAB, where the disruption of self-aggregates and formation of surfactant-induced aggregates take place simultaneously. The disruption of self-aggregates is marked by an increase in fluorescence whereas the formation of surfactant-induced aggregates is marked by a decrease. Their interplay causes ϕ_f to pass through a minimum. Both kinds of aggregates dissociate on micellization [18], and so, ϕ_f increases remarkably at the cmc.

The subtle initial decrease in fluorescence quantum yield with CTAB could be mistaken to be an experimental error, but its genuineness is brought out in the time-resolved measurements. A fluorescence lifetime of 0.13 ns has been obtained at 0.22 mM of CTAB. With further addition of CTAB up to the concentration of 0.4 mM, it keeps decreasing and reaches a value of ~50 ps and thereafter, it starts increasing to a saturation value of 1.9 ns around the cmc (Figs. 5a and 6). In case of SDS, there is no such initial decrease in fluorescence. At an SDS concentration of 1.6 mM, the lifetime of 0.5 ns is obtained and it increases up to 2.3 ns at 8 mM and thereafter it remains unchanged for any further addition of surfactant (Figs. 5b and 6). Thus, the time-resolved experiments confirm the occurrence of premicellar aggregates of purpurin 18, in which its fluorescence is quenched dynamically, for intermediate concentrations of CTAB and their absence for SDS.

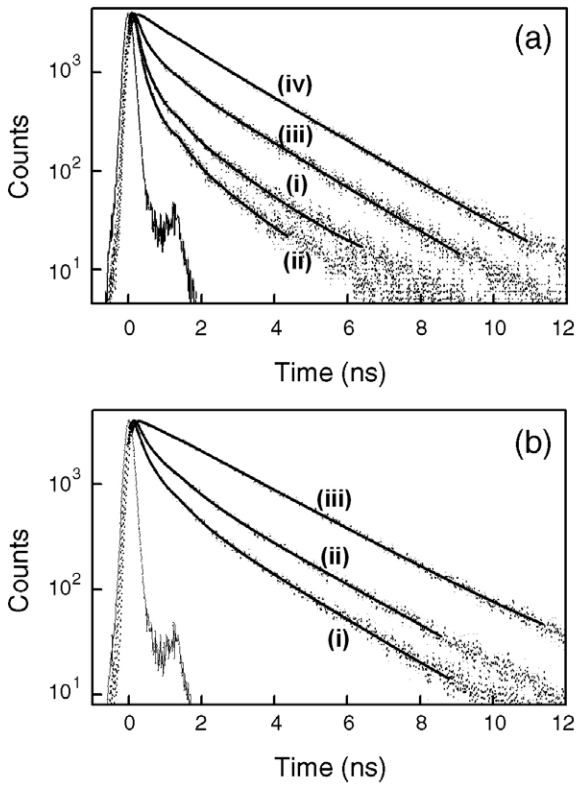

Fig. 5. Fluorescence decays of 7 mM purpurin 18 at different concentrations of (a) CTAB (i) 0.22 mM, (ii) 0.40 mM, (iii) 0.80 mM, (iv) 5.0 mM and (b) SDS (i) 1.6 mM, (ii) 8.0 mM, (iii) 20 mM. λ_{ex} = 406 nm, resolution = 7 ps/ch.

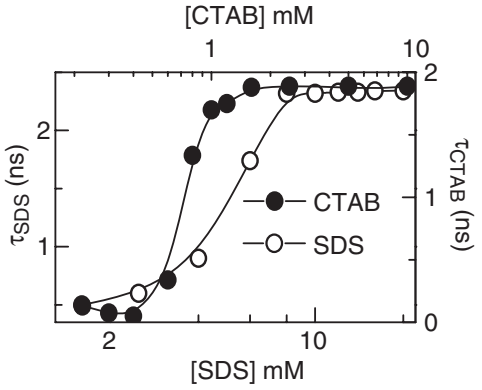

Fig. 6. Variation of fluorescence lifetime of 7 μm purpurin 18 with surfactant concentration. There is a notable dip at low concentrations of CTAB, but with SDS, the lifetimes increase throughout.

The association constants (K_a) obtained from the fits of the optical absorption spectra using Eq. (2) are listed in the Table 1. The K_a for CTAB is found to be more than two hundred times larger than that of SDS. This could be due to the electrostatic assistance to binding between the dye and the surfactant in CTAB and its absence with SDS. The results are in good agreement with the reports by Tabak and coworkers, where the binding constant for anionic $TPPS_4$ at pH 7.5, is larger with cationic surfactant Cetyl trimethyl ammonium chloride (CTAC) in comparison to zwitterionic surfactant *N*-hexadecyl-*N*,*N*-dimethyl-3-ammonio-1-propanesulfonate (HPS), whereas it is the other way around at pH 3.0 [27].

3.2. RLS and DLS studies with CTAB and SDS

We have performed the resonance light scattering (RLS) to monitor the formation of aggregates. In general, in the spectral range where a solution has optical absorption, an increase in scattered light intensity can be observed as a result of the increase of refractive index of the scattering medium in this range (RLS effect) [24]. Usually this increase is masked by absorption; however when aggregates are formed, this effect can be considerably strong as the RLS intensity is proportional to the square of the scattering particle volume. Thus RLS has become an important tool in the study of formation of aggregates [24,25]. Fig. 7 shows the RLS spectra of purpurin 18 in CTAB and SDS micelles. In the absence of surfactants, purpurin 18 exhibits a strong RLS spectrum, having two distinct peaks at 462 nm and 415 nm. Upon addition of CTAB, both the peaks increase initially up to a surfactant concentration of

Table 1
The critical micellar concentrations (cmc), aggregation number (*n*) and the binding constants of purpurin 18 with surfactants

Surfactant	cmc (M)	*n*	K_a (M^{-1})
CTAB	0.9×10^{-3}	170	$(24\pm2)\times10^3$
SDS	8.0×10^{-3}	62	$(1.2\pm0.1)\times10^2$
AOT	4.0×10^{-4}	20	$(2.3\pm0.2)\times10^2$

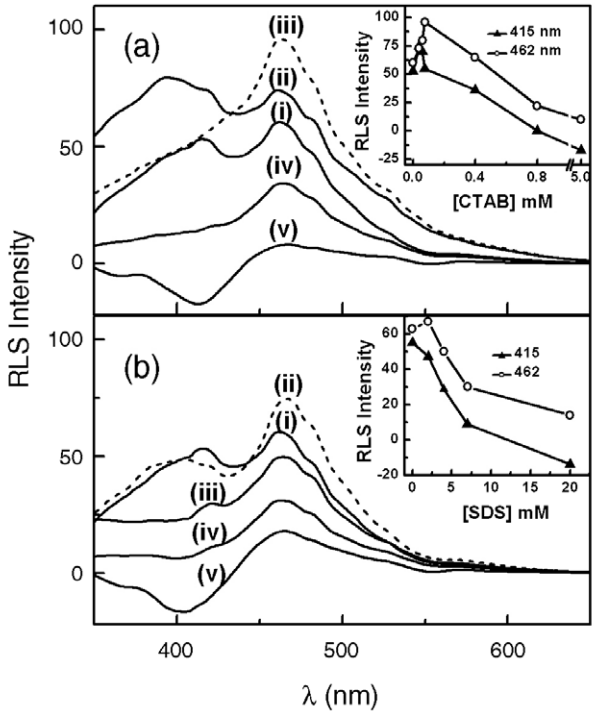

Fig. 7. RLS spectra of 7 mM purpurin 18 at different concentrations of (a) CTAB 0 mM (i), 0.004 mM (ii), 0.076 (iii), 0.8 mM (iv), 5 mM (v) and (b) SDS 0 mM (i), 2 mM (ii), 4 mM (iii), 7 mM (iv), 20 mM (v). The insets show the variation of intensities at 415 nm and 462 nm with surfactant concentration.

0.022 mM, indicating an increase in the extent of aggregation up to this concentration. Thereafter the peak at 415 nm decreases gradually and the peak at 462 nm increases until a CTAB concentration of 0.1 mM, which can be interpreted as the development of a certain kind of aggregate while a different kind of aggregates gets disrupted. This is in agreement, qualitatively, with the formation of surfactant-induced aggregates with CTAB at submicellar concentration. On further increase in surfactant concentration, both the peaks diminish and a trough develops at 402 nm at around the cmc of CTAB. The trough becomes more prominent beyond the cmc and reaches a saturation value at a concentration of 5 mM (Fig. 7a). This is the signature of complete disruption of aggregates of all kinds and formation of monomers, which are incorporated in micelles. In case of SDS, there is a negligible increase in intensity of scattered light. Both the peaks decrease progressively with addition of the surfactant and the trough develops at the same wavelength around the cmc (Fig. 7b). These results are analogous to those of earlier studies of RLS monitoring of aggregation of some water soluble anionic porphyrins, tetraphynylporphinesulfonates ($H_4TPPS_3^-$ and $H_4TPPS_4^{2-}$) in the Soret region at pH 1 by Pasternack and coworkers, which is further assigned as J-aggregates by Akins et al [31,32]. As the peaks obtained are rather broad, in contrast to the above reports, we do not find any spectroscopic signature of ordered aggregates, whereas very sharp peaks are supposed to observe for the highly ordered J-aggregates. However, the RLS results serve to verify one of the major inferences drawn from the absorbance experiments, namely, the difference between the additions of the CTAB and SDS inasmuch as the cationic surfactant induces the formation of new aggregates at lower concentration, whereas the sole effect of the anionic surfactant is to disrupt the aggregates.

DLS has been performed to get the idea of the physical size of the aggregates. In neat buffer the diameters (hydrodynamic diameter) of the aggregates are found to vary in a considerably wide range from 1180 nm to 600 nm, whereas the mean diameter is 1032 nm indicating a larger contribution of large size aggregates. This is in agreement with the inference drawn form the electron microscopy, as described earlier in the report. With addition of CTAB as well as SDS, the mean diameter decreases gradually until it becomes nearly equal to the size of the micelles around the respective cmc values. Though R_h and D vary linearly with increase in SDS concentration, for CTAB, it shows a slight deviation of 0.1 mM from the linear variation. The polydispersity indices (PDI) values are as such quite high for the purpurin 18 aggregates and these become higher with increase in surfactant concentration (Table 2). Even after the cmc of the surfactants, the larger PDI indicates a wide distribution in size of the purpurin 18-incorporated micelles, and this makes the solution less monodisperse.

3.3. Purpurin 18 in AOT reverse micelle

Reverse micelles provide an attractive model system for biomembranes since they mimic a number of important and essential features of biological membranes despite lacking much of the complexity associated with them [33,35]. The highly structured yet heterogeneous water molecules in reverse micelles represent interesting models for those present in biological systems, which have considerably different properties compared to bulk water [34]. In AOT/*n*-heptane reverse micelles, the Soret band at 409 nm shows almost no change (~2 nm) in the peak position with addition of water, whereas the Q band undergoes a red shift from 697 nm to 701 nm, with increase in W_0 value up to 32, where W_0 is the molar ratio between the water and surfactant in the system ($W_0 = [H_2O]/[AOT]$). Both the bands show a decrease in absorbance with increase in W_0 values (Fig. 8a). These changes in the absorption spectra with water content clearly indicate that the fluorophore binds to the reverse micelle. No changes would

Table 2
The variation of hydrodynamic diameter (R_h), diffusion coefficient (D) and polydispersity indices (PDI) with surfactant concentration

[CTAB] mM	PDI	$D\times10^6$ ($cm^2\ s^{-1}$)	R_h (nm)	[SDS] mM	PDI	$D\times10^6$ ($cm^2\ s^{-1}$)	R_h (nm)
0	0.566	0.006	1032±42	0	0.566	0.006	1034±41
0.004	0.578	0.008	754±33	1	0.571	0.007	819±38
0.076	0.612	0.010	618±26	2	0.593	0.009	653±27
0.10	0.643	0.008	780±37	6	0.632	0.015	376±18
0.40	0.629	0.016	359±19	8	0.667	0.030	187±13
1.00	0.687	0.048	121±12	10	0.691	0.062	93±8
5.00	0.611	0.475	12±3	20	0.642	0.380	15±3

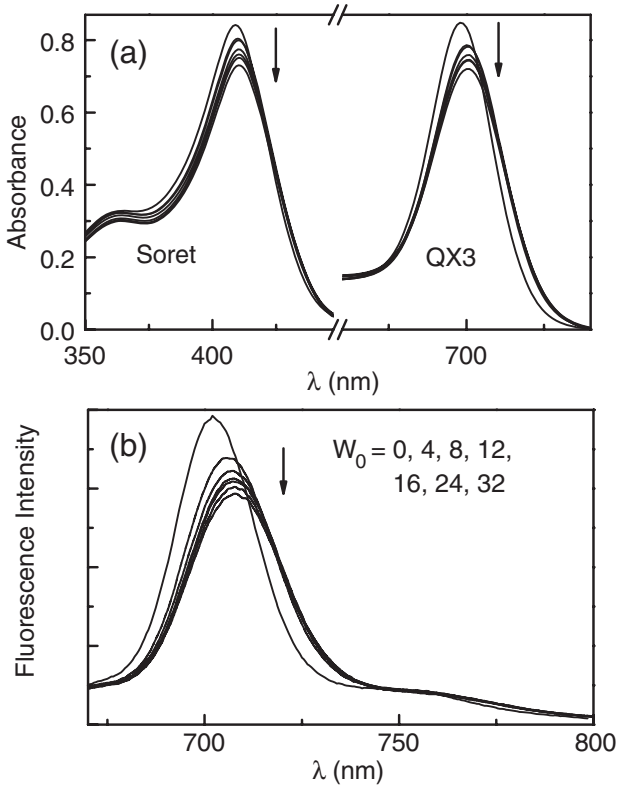

Fig. 8. (a) Absorption and (b) fluorescence spectra of 7 μM purpurin 18 in AOT reverse micelles with varying the water contents (W_0=0, 4, 8, 12, 16, 24, 32). The Q band has been magnified by a factor of 3 for the sake of clarity.

have been observed, if they would reside in the bulk apolar solvent.

The fluorescence emission spectra in reverse micelles at different values of W_0 are shown in Fig. 8b. The emission maximum in the absence of water is at 700 nm. The blue shift of 10 nm with respect to aqueous micelles indicates that the overall polarity experienced by purpurin 18 in reverse micelles is significantly lower than that experienced in CTAB or SDS micelles.

The fluorescence intensity decreases with a red shift of 8 nm with the first addition of water, indicating an increased polarity experience by the fluorophore upon increasing the water content of the reverse micelle. This is an additional evidence for binding of purpurin 18 to the reverse micelle, at least in the presence of the water pool. No change in the spectral properties of the fluorophore would have been observed with addition of water if it would not have been associated with the reverse micelle. We find that the radiative rates are more or less the same, but the nonradiative rates increase upon addition of water (Table 3). This is the characteristic observation for fluorophores that come in contact with the water pool [35]. Thus, we find that purpurin 18 comes in contact with the water pool in the microemulsion. The association constant in reverse micelles is calculated in the same way as for micelles and turns out to have a value that is smaller than that of CTAB, but larger than SDS (Table 1). Now, the question is whether the fluorophores are located in the water pool or the interface. This question can be addressed through fluorescence quenching studies, as a close proximity between

Table 3
Spectral and temporal properties of the fluorescence of purpurin 18 as a function of W_0 in AOT reverse micelles

W_0	ϕ_f	τ_f (ns)	$k_R \times 10^8$ s^{-1}	$k_{NR} \times 10^8$ s^{-1}
0	0.230	2.30	0.99	3.3
4	0.223	2.25	0.99	3.5
8	0.216	2.20	0.99	3.6
12	0.213	2.15	1.00	3.7
16	0.212	2.10	1.01	3.8
24	0.207	2.00	1.05	4.0
32	0.202	1.90	1.10	4.2

the fluorophore and the quencher is a requirement for quenching and so, quenching by hydrophobic quenchers are more efficient for fluorophores that are located in the surfactant/bulk phase interface, rather than those in the water pool [36]. We observe that phenothiazine can successfully quench the fluorescence of purpurin 18. As this quencher stays preferably in the surfactant–bulk phase interface, we conclude that purpurin 18 also resides in the same region. Moreover, the Stern–Volmer plot exhibits an upward curvature, indicating more than one types of quenching to be operative (Fig. 9). The radiative lifetime decreases from 2.3 ns to 1.9 ns upon addition of the quencher. The linear Stern–Volmer plot from the fluorescence lifetime indicates some extent of dynamic quenching by the phenothiazine molecules, with a bimolecular quenching constant of 8×10^4 M^{-1} s^{-1}, which is smaller than that obtained from the slope of the Stern–Volmer plot obtained from the fluorescence quantum yields. This indicates that a significant amount of the quenching is static in nature and serves as a pointer to the formation of association complexes of phenothiazine and purpurin 18, which in turn corroborates our contention about the location of the fluorophore in the interfacial region. This could be important in serving as a model for the location drugs, analogous to purpurin 18, in cells, which are modeled by the microemulsions. From the present results, one could propose that such drugs, upon incorporation in cells, would prefer to be located in the membrane rather than in the cytoplasm. This could be of profound implication in the application of such drugs in PDT. However, it must be noted that such a hypothesis would be rather simplistic, as the situation could be way more complicated in the real cells.

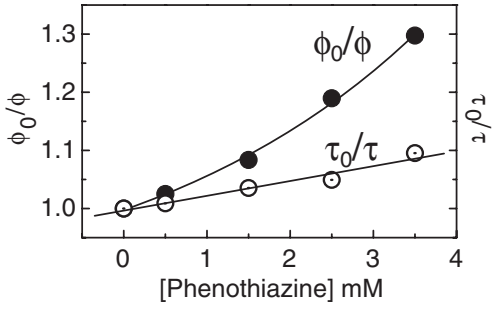

Fig. 9. The Stern–Volmer plot for steady state and time-resolved parameters for quenching of fluorescence of 7 μM purpurin 18 by phenothiazine in AOT reverse micelles with W_0=32.

3.4. Interaction with HSA

The aim to investigate further the interaction of purpurin 18 and HSA, a transport protein in blood plasma and known to bind a variety of therapeutic drugs, is to get an idea of probing it as a potential anti-tumor drug. The interaction of a large number of other porphyrins with bovine serum albumin, human serum albumin and other related proteins is reported earlier and the binding properties are studied by using different techniques [1,3,5,14,37,38]. As mentioned earlier, the absorption spectrum of purpurin 18 comprises a strong aggregate peak at 758 nm in PBS (pH 7.4). With addition of HSA, the monomer peak develops at 705 nm, as with CTAB and SDS, indicating the disruption of the aggregates. The deaggregation begins at an HSA concentration of 0.75×10^{-6} M, which is ten times less than the concentration of purpurin 18. This is marked by the onset of fluorescence, which is not perceivable for lower HSA concentration. With an increase in the concentration of HSA, the monomer peak becomes more prominent at the expense of the aggregate peak (Fig. 10a). Two clear isobestic points at 725 nm and 442 nm indicate equilibrium between the aggregated and the monomeric/bound forms of purpurin 18. There is a continuous increase in fluorescence quantum yield with the concentration of the albumin. Unlike with the surfactants, the aggregate peak does not disappear completely, even for a concentration of HSA as high as 1×10^{-4} M, which is 14 times more than the fluorophore. Both the peaks at 758 nm and 705 nm get saturated as the concentration of HSA of 45×10^{-6} M, which is about 6.5 times the concentration of fluorophore (Fig. 10b). Similar results are also obtained with 3 μM purpurin 18. Thus, it seems that the disruption of the aggregates by HSA is not complete, even at very low concentrations of the fluorophore and that purpurin 18 binds to HSA partly in monomeric and partly in aggregated form. For a number of porphyrin, the complete deaggregations by proteins have been widely reported earlier [37,38]. No change in fluorescence lifetime is observed, indicating that once the monomers are formed, they do not experience any further change in the microenvironment. In the Chipman plot, the nonlinearity of the plot indicates the presence of more than one chlorin binding sites in HSA (Fig. 11), because for single binding side, the Chipman plot is supposed to be a straight line with a liner fit [28,29]. As described in the Experimental section, the absorbance at infinite concentration of HSA has been calculated by plotting $A_0/\Delta A$ vs. $[\mathrm{HSA}]^{-1}$ (Fig. 11, inset). The intersection of the plot and the line drawn from the zero abscissa gives the binding constant K_b, which is estimated to be 3.4×10^5 M^{-1}. The binding constants for some other porphyrins with HSA have been reported to vary in the order of 10^4 to 10^8, depending on various factors like the nature/charge of the porphyrin, the nature of the protein and the nature of the local environment as well [28,29,37,38]. The binding constant is also calculated from the fluorescence data in the same way and the value obtained is within 5% of that obtained from the absorption results. Another reason that might complicate the Chipman plot is the existence of the aggregates, which can considerably interfere with the construction of the plot.

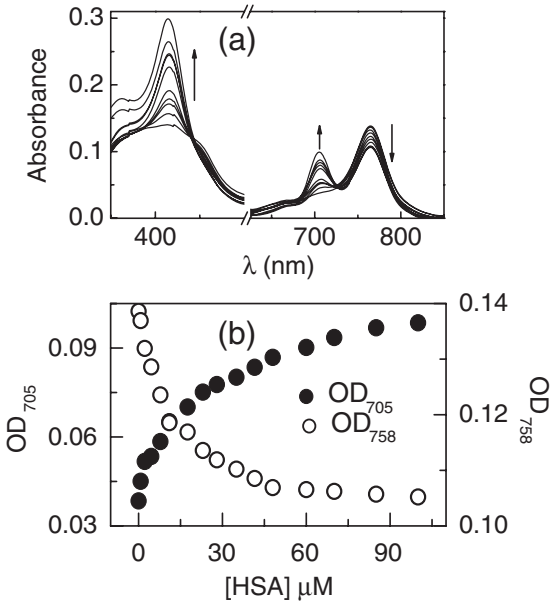

Fig. 10. (a) Absorption spectra of 7 μM purpurin 18 and (b) variation of absorbance at 705 nm and 758 nm at different concentrations of HSA (0 to 100 mM).

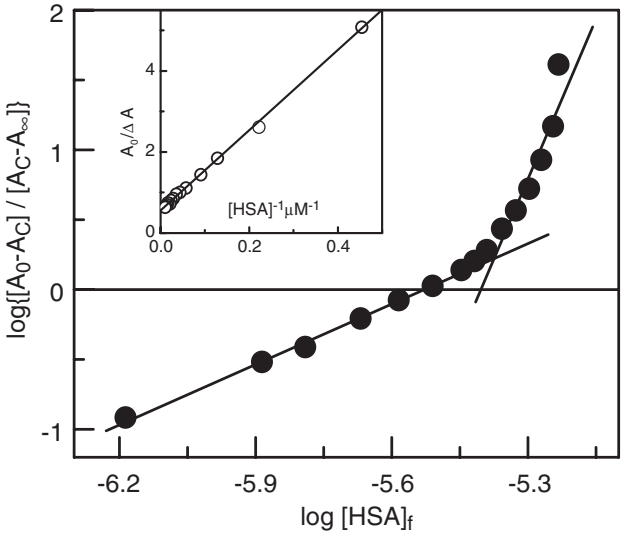

Fig. 11. The Chipman plot for calculation of the binding constant of 7 μM purpurin 18 with HSA. The inset shows the plot of A_0/Δ_0 vs. $[\mathrm{HSA}]^{-1}$, from this A_∞ has been calculated.

4. Conclusion

Surfactants are found to induce complete disruption of the purpurin 18 aggregates in PBS at pH 7.4. In case of reverse micelles, no aggregates are observed at all, since the apolar phase is present in large excess and solubilizes purpurin 18 preferentially. The fluorophore is found to reside at the interfacial region. HSA is found to bind purpurin 18 in two different sites, but with only a partial disruption of the aggregates. Absorption and fluorescence experiments are

found to be in agreement with each other on the presence of equilibrium between momomeric and aggregated forms of purpurin 18. A possible implication of this study in photodynamic therapy is that even though hydrophobic molecules like purpurin 18 can be expected to remain aggregated in the blood stream, it can be expected that the aggregates get disrupted when they are taken up by cells and so, in the cells, they might be expected to exist as monomers, which usually possess a greater photodynamic efficacy than aggregates. In vitro studies with purpurin 18 are underway to explore this aspect more closely.

Acknowledgement

This work is supported by CSIR research grant no. 01 (1851)/03/EMR-II.

References

[1] P.C. de Smidt, A.J. Versluis, T.J. van Berkel, Properties of incorporation, redistribution, and integrity of porphyrin–low-density lipoprotein complexes, Biochemistry-US 32 (1993) 2916–2922.
[2] J. Moan, Q. Peng, J.F. Evensen, K. Berg, A. Western, C. Rimington, Photosensitizing efficiencies, tumor- and cellular uptake of different photosensitizing drugs relevant for photodynamic therapy of cancer, Photochem. Photobiol. 46 (1987) 713–721.
[3] B. Roeder, D. Naether, T. Lewald, M. Braune, C. Nowak, W. Freyer, Photophysical properties and photodynamic activity in vivo of some tetrapyrroles, Biophys. Chem. 35 (1990) 303–312.
[4] A. Datta, A. Dube, B. Jain, A. Tiwari, P.K. Gupta, The effect of pH and surfactant on the aggregation behavior of chlorin p6: a fluorescence spectroscopic study, Photochem. Photobiol. 75 (2002) 488–494.
[5] M. Sharma, A. Dube, H. Bansal, P.K. Gupta, Effect of pH on uptake and photodynamic action of chlorin p_6 on human colon and breast adenocarcinoma cell lines, Photochem. Photobiol. Sci. 3 (2004) 231–235.
[6] K. Das, B. Jain, A. Dube, P.K. Gupta, pH dependent binding of chlorin-p_6 with phosphatidyl choline liposomes, Chem. Phys. Lett. 401 (2005) 185–188.
[7] P.P.S. Lee, T. Ngai, J.D. Huang, C. Wu, W.P. Fong, D.K.P. Ng, Synthesis, characterization, biodegradation, and in vitro photodynamic activities of silicon(IV) phthalocyanines conjugated axially with poly(β-caprolactone), Macromolecules 36 (2003) 7527–7531.
[8] K. Abata, K. Fukushima, K. Oda, I. Okura, Selective aggregation of zinc phthaloc-yanines in the skin, J. Porphyr. Phthalocyanines 4 (2000) 278–284.
[9] T. Ohyama, H. Mita, Y. Yamamoto, Binding of 5,10,15,20-tetrakis(*N*-methylpyridinium-4-yl)-21*H*,2,3*H*porphyrin to an AT-rich region of a duplex DNA, Biophys. Chem. 113 (2005) 53–59.
[10] N.C. Maiti, S. Mazumdar, N. Periasamy, J- and H-aggregate of porphyrin–surfactant complexes: time-resolved fluorescence and other spectroscopic studies, J. Phys. Chem., B 102 (1998) 1528–1538.
[11] A.S.R. Koti, N. Periasamy, Cyanine induced aggregation in meso-tetrakis (4-sulphonatophenyl) porphyrin anions, J. Mater. Chem. 12 (2002) 2312–2317.
[12] H. Kano, T. Saito, T. Kobayashi, Observation of Herzberg–Teller-type wave-packet motion in porphyrin J-aggregates studied by sub-5-fs spectroscopy, J. Phys. Chem., A 106 (2002) 3445–3453.
[13] G. Jori, E. Reddi, The role of lipoproteins in the delivery of tumour-targeting photosensitizers, Int. J. Biochem. 25 (1993) 1369–1375.
[14] A. Mazzaglia, N. Angelini, R. Darcy, R. Donohue, D. Lombardo, N. Micali, M.T. Sciortino, V. Villari, L.M. Scolaro, Novel heterotopic colloids of anionic porphyrins entangled in cationic amphiphilic cyclodextrins: spectroscopic investigation and intracellular delivery, Chem. Eur. J. 9 (2003) 5762–5769.
[15] W.D. Jang, N. Nishiyama, G.D. Zhang, A. Harada, D.L. Jiang, S. Kawauchi, Y. Morimoto, M. Kikuchi, H. Koyama, T. Aida, K. Kataoka, Supramolecular nanocarrier of anionic dendrimer porphyrins with cationic block copolymers modified with polyethylene glycol to enhance intracellular photodynamic efficacy, Angew. Chem., Int. Ed. Engl. 44 (2005) 419–423.
[16] C.M. Pitsillides, E.K. Joe, X. Wei, R.R. Anderson, C.P. Lin, Selective cell targeting with light-absorbing microparticles and nanoparticles, Biophys. J. 84 (2003) 4023–4032.
[17] P.J. Wood, J.M. Sansom, K. Newell, I.F. Tannock, I.J. Stratford, Reduction of tumour intracellular pH and enhancement of melphalan cytotoxicity by the ionophore Nigericin, Int. J. Cancer 60 (1995) 264–268.
[18] P.P. Mishra, J. Bhatnagar, A. Datta, Fluorescence monitoring of pH dependent complexation of chlorin p6 with surfactants, Chem. Phys. Lett. 386 (2004) 158–161.
[19] S. Patel, A. Datta, pH effect on the binding of chlorin derivatives with cremophor EL, a potential drug delivery vehicle, Chem. Phys. Lett. 413 (2005) 31–35.
[20] M. Schmidt, E.-W. Knapp, Accurate pK_a determination for a heterogeneous group of organic molecules, ChemPhysChem 5 (2004) 1513–1522.
[21] J.K. Hoober, T.W. Sery, N. Yamamoto, Photodynamic sensitizers from chlorophyll: purpurin-18 and chlorin p6, Photochem. Photobiol. 48 (1988) 579–581.
[22] S. Das, A. Datta, K. Bhattacharya, Deuterium isotope effect on 4-aminophthalimide in neat water and reverse micelles, J. Phys. Chem., A 101 (1997) 3299–3304.
[23] P.G. Seybold, M. Gouterman, Porphyrins XIII: fluorescence spectra and quantum yields, J. Mol. Spectrosc. 31 (1969) 1–13.
[24] R.F. Pasternack, P.J. Collings, Resonance light scattering: a new technique for studying chromophore aggregation, Science 269 (1995) 935–939.
[25] P.J. Collings, E.J. Gibbs, T.E. Starr, O. Vafek, C. Yee, L.A. Pomerance, R. F. Pasternack, Resonance light scattering and its application in determining the size, shape, and aggregation number for supramolecular assemblies of chromophores, J. Phys. Chem., B 103 (1999) 8474–8481.
[26] J.R. Perussi, V.E. Yushmanov, S.C. Monte, H. Imasato, M. Tabak, Interaction of premaquine and chloroquine with ionic micelles as studied by 1H NMR and electronic absorption spectroscopy, Physiol. Chem. Phys. Med. NMR 27 (1995) 1–15.
[27] S.C.M. Gandini, V.E. Yushmanov, I.E. Borissevitch, M. Tabak, Interaction of the Tetra(4-sulfonatophenyl) porphyrin with ionic surfactants: aggregation and location in micelles, Langmuir 15 (1999) 6233–6243.
[28] D.M. Chipman, V. Grisaro, N. Sharon, The binding of oligosaccharides containing *N*-acetylglucosamine and *N*-acetylmuramic acid to lysozyme, J. Biol. Chem. 242 (1967) 4388–4394.
[29] N.A.M. Sultan, B.G. Maiya, M.J. Swamy, Theromodynamic analysis of porphyrin binding to momordica charantia (bitter ground) lectin, Eur. J. Biochem. 271 (2004) 3274–3282.
[30] S.S. Berr, M.J. Coleman, M. Jones, J.S. Johnson, Small-angle neutron scattering study of the structural effects of substitution of tetramethylammonium for sodium as the counterion in dodecyl sulfate micelles, J. Phys. Chem. 90 (1986) 6492–6499.
[31] R.F. Pasternack, P.R. Huber, P. Boyd, G. Engasser, L. Francesconi, E.J. Gibbs, P. Fasella, G.C. Venturo, L.D.C. Hinds, On the aggregation of mesosubstituted water-soluble porphyrins, J. Am. Chem. Soc. 94 (1972) 4511–4517.
[32] D.L. Akins, H.R. Zhu, C. Guo, Absorption and Raman scattering by aggregated meso-tetrakis(*p*-sulfonatophenyl)porphine, J. Phys. Chem. 98 (1994) 3612–3618.
[33] Y. Ikushima, Supercritical fluids: an interesting medium for chemical and biochemical processes, Adv. Colloid Interface Sci. 71 (1997) 259–263.
[34] K. Bhattacharyya, B. Bagchi, Slow dynamics of constrained water in complex geometries, J. Phys. Chem., A 104 (2000) 10603–10613.
[35] A. Datta, D. Mandal, S. Pal, K. Bhattacharyya, Intramolecular charge transfer processes in confined systems: Nile red in reverse micelles, J. Phys. Chem., B 101 (1997) 10221–10225.
[36] J. Yu, X. Wang, B. Zhang, J. Chen, L. Zhang, Y. Weng, Y. Cao, Amphiphilic porphyryns in reverse micelles: the influence of the molar

ratio of water to surfactant and side-chain length on their triplet-state lifetimes. A case study, Phys. Chem. Chem. Phys. 5 (2003) 3660–3665.
[37] S.M. Andrade, S.M.B. Costa, Spectroscopic studies on the interaction of water soluble porphyrin and two drug carrier proteins, Biophys. J. 82 (2002) 1607–1619.
[38] T.T. Tominaga, V.E. Yusbmanov, l.E. Borissevitch, H. Imasato, M. Tabak, Aggregation phenomena in the complexes of iron tetraphenylporphine sulfonate with bovine serum albumin, J. Inorg. Biochem. 65 (1997) 235–244.